Chapter 4: Investigation of Dielectric Properties of Fluoride-Mediated, Pure-Silica Zeolite Thin Films

Abstract

The fluoride-mediated synthesis of pure-silica zeolite thin films with the CHA, STT, ITW and -SVR topologies on surface-modified (100) Si wafers is reported. The films are prepared using the vapor phase transport of the fluoride mineralizing agent, a method used previously to make thin films of the pure-silica zeolite topology LTA. The CHA, STT, ITW, and -SVR films are polycrystalline, intergrown, continuous, and well-adhered to their substrates. The films are characterized by a combination of techniques, including X-ray diffraction and field emission scanning electron microscopy. The fluoride-mediated, pure-silica LTA, CHA, STT, ITW, and -SVR zeolite powders and films are investigated for low dielectric constant (low-*k*) material applications. This investigation demonstrates not only that these materials are appropriate for low-*k* applications, especially the LTA topology, which has the lowest intrinsic dielectric constant of all the pure-silica zeolites, but also shows interesting dielectric behavior with respect to porosity. All the zeolites investigated here, except STT, give *k*-values lower than predicted from their structures using the Bruggeman effective medium model, which has been commonly employed and found able to predict dielectric constants of amorphous silicas. This marks an inherent difference between zeolites and other porous silicas, and suggests the potential to tailor the dielectric properties based on not only porosity, but also pore architecture.

Reproduced in part with permission from H. K. Hunt, C. M. Lew, M. Sun, Y. Yan and M. E. Davis, Pure-Silica LTA, CHA, STT, ITW, and -SVR Thin Films and Powders for Low-k Applications, submitted to *Microporous Mesoporous Mat*. 2009.

1. Introduction

As feature sizes in integrated circuits continue to decrease, a corresponding increase in energy dissipation, resistance-capacitance delay, and cross-talk noise is expected to become a significant issue for microprocessors.[1,2] To combat this, the semiconductor industry must develop a replacement for the traditional dense silica dielectric material used to insulate the wiring between transistors. According to the International Technology Roadmap for Semiconductors 2007 Edition – Interconnect, an ultra-low dielectric material with an effective k between 2.3 and 2.6 (in comparison to $k \sim 4$ for dense silica) is needed to accommodate an integrated circuit with feature sizes of 14 nm or smaller by 2020.[1] Additionally, this new material must be capable of integration with current fabrication processes, and must withstand normal operation conditions. These requirements restrict the types of materials that may be useful for this application. For instance, to integrate with the interconnect fabrication processes, the dielectric material must have mechanical and chemical properties similar to silica, such as an elastic modulus greater than 6 GPa to survive chemical and mechanical polishing, a high fracture toughness to prevent cracking, thermal expansion coefficients similar to that of the metal interconnects to reduce failure during thermal cycling, and lastly, high chemical and thermal stability to avert dielectric degradation or decomposition.[3,4,5] It is for these reasons that the general approach to finding new low-k materials involves investigating both their electronic and physicochemical properties.

The familiar parallel-plate capacitor is shown in Figure 4.1, with a dielectric medium between the two plates. A dielectric material for capacitive applications is ideally electrically non-conductive, but easily polarized, as this allows the medium to store energy through polarization when an electric field is applied. Polarization induces a net charge density on the plates of the capacitor, and therefore increases the charge storage capacity of a capacitor. Dielectric materials are also useful, as mentioned above, for insulating current-carrying conductors. The dielectric constant, also known as the relative permittivity, of a dielectric medium is a measure of the relative increase in the capacitance of a capacitor when the insulation between the two plates is changed to a dielectric medium from vacuum. The capacitance equation is then given by Equation 4.1, where C is the capacitance, ε is the permittivity, A is the plate area, and d is the separation between plates. The permittivity is defined as the relative permittivity (symbolized by either *k*, as used in the microelectronic industry, or ε_r, as used in the scientific community) multiplied by the permittivity of free space (ε_0), as shown in Equation 4.2.

$$C = \frac{\varepsilon A}{d} \qquad \textbf{4.1}$$

$$\varepsilon = \kappa \varepsilon_0 \qquad \textbf{4.2}$$

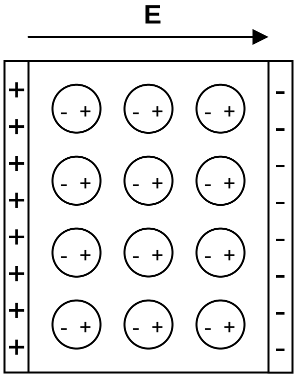

Figure 4.1 Cartoon of a parallel-plate capacitor with a dielectric medium polarized by an electric field, **E**

Typically, the intrinsic dielectric constant of a material is calculated from parallel-plate capacitance measurements and Equations 4.1 and 4.2, as shown in Figure 4.2a, obtained at a specific frequency (usually 1 MHz, as this is similar to operation conditions) using an LCR meter. This measurement is generally carried out under flowing, dry argon to prevent accumulation of water in the sample, which has been shown to increase the dielectric constant of materials with even a slight hydrophilicity. For additional prevention of water adsoption, the surface of the materials may be capped to prevent water adsorption; for instance, it is common to cap silicate materials using a vapor-phase silylation procedure.[6] Parallel-plate capacitance measurements are very straightforward, but have the disadvantage of requiring perfect parallelism via the preparation of high quality, thin films or sheet-like structures, in the metal-insulator-metal structures to obtain consistent and accurate capacitance measurements. An alternative method is time-domain reflectometry (TDR), in which it is coupled with a transmission line, as shown in Figure 4.2b. TDR is generally used to assess impedance variations along transmission lines such as cables, connectors, or circuit boards, and has been shown to be useful for studying small quantities of powders for both high- and low-*k* applications. This method avoids the necessity of creating perfect thin films of materials, which often requires very expensive chemical or mechanical polishing equipment, and can be used to rapidly screen new materials.

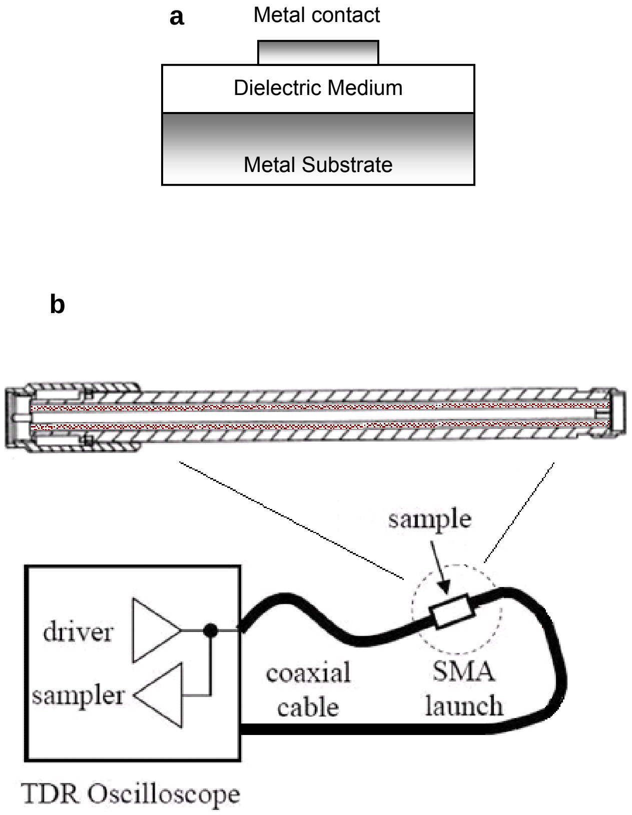

Figure 4.2 (a) Metal-insulator-metal structures used for parallel-plate capacitance measurements; (b) Schematic of a time-domain reflectometer (TDR) coupled with transmission line for dielectric measurements of powder samples (used with permission)[7]

A material's relative permittivity may also be predicted from the polarization properties of its constituent molecules. For instance, the phenomenological Debye equation, which describes the relationship between the dielectric constant (relative permittivity) of a material, and its characteristic properties (the density of molecules, and their response to an applied electric field, measured by their polarizability), is often used as a guideline for the selection of materials with appropriate electronic properties.[2] For instance, the dielectric constant of the material is increased if the molecules in the material have either a permanent dipole moment or an easily induced dipole moment. The ability of molecules to become polarized in an electric field, and thus gain a dipole moment, can be a result of the ease with which ionic polarization or electronic polarization (or frequently both) occurs. The former polarization phenomenon describes the compression or expansion of molecular bond lengths as their nuclei are shifted in response to an applied electric field, while the latter polarization phenomenon relates to the movement of the cloud of bound electrons around their nucleus under an applied electric field. Polar molecules may also undergo orientation polarization, which describes the movement or reorientation of entire molecules in response to the field. In materials not composed of single crystals, interfacial polarization may also play a role in determining polarization. This phenomenon occurs at the interface between two materials, such as grain boundaries, crystal defects, impurities, etc. The Debye equation, which relates these microscopic polarization phenomena to macroscopic relative permittivity, is given in Equation 4.3. N is the number density of molecules in the material, α_e is the electronic polarization of the molecules, α_i is the ionic polarization of the molecules, μ is the orientation polarization of the molecules, k is the Boltzmann constant, and T is the temperature in Kelvin.

$$\frac{\kappa - 1}{\kappa + 1} = \frac{N}{3\varepsilon_0}\left(\alpha_e + \alpha_i + \frac{\mu^2}{3kT}\right) \qquad \textbf{4.3}$$

In cases where the material is composed of molecules without a permanent dipole, like pure silicas, the polarizability of the material then depends solely on the ease with which a dipole moment is induced, as well as the density of molecules in the material, and Equation 4.3 reduces to the well-known Clausius-Mossotti equation (Equation 4.4).

$$\frac{\kappa - 1}{\kappa + 1} = \frac{N}{3\varepsilon_0}\left(\alpha_e + \alpha_i\right) \qquad \textbf{4.4}$$

In general, the development of low-*k* materials focuses on reducing either the ionic and electronic polarizabilities. This is accomplished by modifying the material composition such that ionic bonds and electron density in the material are reduced, or by decreasing the density of the molecules in the material by introducing porosity into the material. The former approach uses either non-silica materials (such as non-polar organic polymers with fluoride or fluorocarbon substitution, and highly fluorinated carbonaceous compounds), or organosilicates (such as organic-inorganic silsesquioxane polymers, and fluorinated silicas).[8,9,10,11,12,13] In these materials, replacing an Si-O bond with Si-CH_3 or Si-F reduces the polarizability of the material, as does the insertion of C-C bonds. The leading approach to *k* reduction, however, is the introduction of porosity into pure-silica materials, organosilicates, or organic polymers.[14,15] This is due, in part, to the widespread use of porous silica-based materials in other industries, such as catalysis, separation, desiccation, etc., and in part to the well-understood methods of manufacturing porosity in silica, such as sol-gel processes, surfactant-templating, and zeolite crystallization.[16] Using this approach, the electronic properties of the base material can be modified in relation to the amount of porosity introduced into the material.

Potential low-*k* materials, however, must also meet the processing requirements as mentioned above. Low-*k* materials based on organic polymers and organosilicates have very attractive electronic properties for low-*k* applications, but often suffer from poor chemical and thermal stability, as well as high coeffecients of thermal expansion when compared with metal interconnects.[3,5] Porous, pure-silica materials, on the other hand, have high chemical and thermal stability when compared with the aforementioned classes of materials, due to their chemical composition.[6,17,18] However, their mechanical properties frequently depend on how the porosity in the material is generated. For example, sol-gel processing or surfactant-templating often result in silica materials with poor mechanical strength due to their lack of crystallinity, and high hydrophilicity, due to a high number of silanol defects.[2,3,19] Materials with low mechanical stiffness, as determined by the elastic modulus, often have questionable ability to survive the chemical mechanical processing (CMP) necessary for integrated circuit fabrication. Hydrophilic materials adsorb water at ambient conditions, which significantly increases the effective *k* of the material (the dielectric constant of water ~ 80). These issues make many of the materials prepared by these porosity-inducing processes unsuitable for low-*k* applications, despite their excellent insulating properties.

Pure-silica zeolites (PSZ), in contrast, have all the aforementioned chemical and mechanical properties necessary to withstand CMP, due to their unique crystalline, microporous structures. This is especially true when fluoride is used as the mineralizing agent, as this generates materials with a low silanol defect density.[18] Additionally, the porosities of these zeolites are easily quantified based on their Framework Density (FD), which is the number of tetrahedrally coordinated atoms per 1000 Å^3, as compared to other types of porous silicas, leading to a quantitative expression of the relationship between zeolite porosity and the resulting dielectric constant. For instance, the LTA topology first produced in pure-silica form by Corma et al. in 2004 has the lowest framework density (FD = 14.2) among all available pure-silica zeolites, and therefore could have the lowest dielectric constant.[20,21] Finally, the abundance of zeolite topologies and hence porosities, allows for the investigation of the effects of not only porosity, but also the pore structure, on the *k*-value, as several pure-silica zeolites with framework densities in the range of interest for low-*k* materials (FD = 14.2 – 19) have similar framework densities, but very different pore structures. If pore structure does play a role in determining the dielectric constant of zeolites, then the ability to tune this parameter, in addition to porosity, could provide materials that are significant improvements over other types of porous silicas. For these reasons, pure-silica zeolites have been suggested as excellent candidates for low-*k* materials.[22]

Of the 19 known pure-silica zeolites, the intrinsic dielectric constant of only five (MFI, (FD = 18.4, $k = 2.7$ via *in situ* crystallization), MEL (FD = 17.4, $k = 1.9$ via spin-coating), *MRE (FD = 19.8, $k = 2.7$ via traditional vapor phase transport), BEA* (FD = 15.3, $k =$

2.3 via *in situ* crystallization, and 2.07 via secondary growth), and LTA (FD = 14.2, k = 1.69 via *in situ* crystallization) have been studied as low-*k* materials via thin film techniques.[4,23,24,25,26,27] This was caused by both limitations in the traditional methodology required to produce pure-silica zeolite thin films with low silanol defect density, and the necessity of obtaining perfect parallel-plate structures from which the *k*-value of the film may be determined.[6,27,28,29] Recently, we presented new techniques for both the dielectric characterization of pure-silica zeolite powders, which permits us to screen the dielectric properties of pure-silica zeolites without the necessity of creating parallel-plate structures from thin films,[7] and the synthesis of fluoride-mediated, pure-silica zeolite thin films, which allows us to expand the library of pure-silica topologies available as films.[30] The former technique used Time Domain Reflectometry (TDR), in conjunction with a transmission line, as shown in Figure 4.2b, to evaluate the *k*-value for pure-silica zeolite powders. TDR can measure the dielectric constant of powder samples in a large frequency range very rapidly with only a small amount (~ 300 mg) of sample, and is believed to be applicable to high-*k* materials, as well as low-*k* materials. Simultaneously, we developed a Vapor Phase Transport of Fluoride (VPTF) method to generate thin films of fluoride-mediated pure-silica zeolites; this method was demonstrated by producing thin films of LTA on a variety of substrates.[30] These techniques enable us to investigate several new, pure-silica zeolites in the porosity range of interest for low-*k* materials and to compare them with known materials. Here, we present the thin film synthesis of pure-silica zeolites CHA (FD = 15.1), STT (FD = 17.0), ITW (FD = 17.7), and –SVR (FD = 17.2) using the VPTF, and the results of an investigation of the electronic properties of the fluoride-mediated, pure-silica LTA, CHA, STT, ITW, and -SVR materials as they relate to their porosity and pore structure.[31,32,33,34]

Five pure-silica zeolite materials are investigated in this report: LTA, CHA, ITW, STT, and -SVR. The unit cell structures of the five materials are shown in Figure 4.3a-e. These five materials are chosen because each is a material potentially useful in low-*k* applications, due to their relatively low framework density, and in other applications, such as catalysis, separation, membrane reactors, chemical sensors, etc., applications. For instance, PSZ LTA (FD = 14.2) has the lowest framework density of all the pure-silica zeolites, and not only should have the lowest dielectric constant, but it should also be useful as a material for a high-flux membrane due to its open framework.[35] PSZ CHA (FD = 15.1) has been suggested for the adsorption and separation of organics, as well as for the storage of hydrogen and methane.[31] Similarly, PSZ ITW (FD = 17.7) has shown an ability to selectively adsorb propene from a propane / propene mixture, and therefore may be used as an adsorbent for pressure swing adsorbers.[32,36] PSZ STT (FD = 17.0) is a frequent result of PSZ CHA syntheses crystallized over long times due to the non-selectivity of the structure-directing agent, N,N,N-trimethyladamantammonium hydroxide, and is unique in that it has two types of pore channels, one defined by nine-member rings, and the other defined by seven-member rings.[34] Lastly, PSZ -SVR (FD = 17.2), may have intriguing possibilities for gas separation, due to its three-dimensional 10-member ring pore system and periodic Si vacancy, and has shown to be a good catalyst when made as a high-silica zeolite.[33] Some of the applications described above may require zeolites in planar (thin film or membrane) form. Films and membranes are often synthesized through the use of colloidal zeolite suspensions and nanoparticles, but these methods are generally unsuited for the synthesis of these pure-silica zeolites, as they are made via the fluoride route. Therefore, we are interested in demonstrating that these zeolites can be synthesized into thin films as well as powders, and then investigating their dielectric properties to determine if not only porosity, but also pore structure, influence their *k*-value.

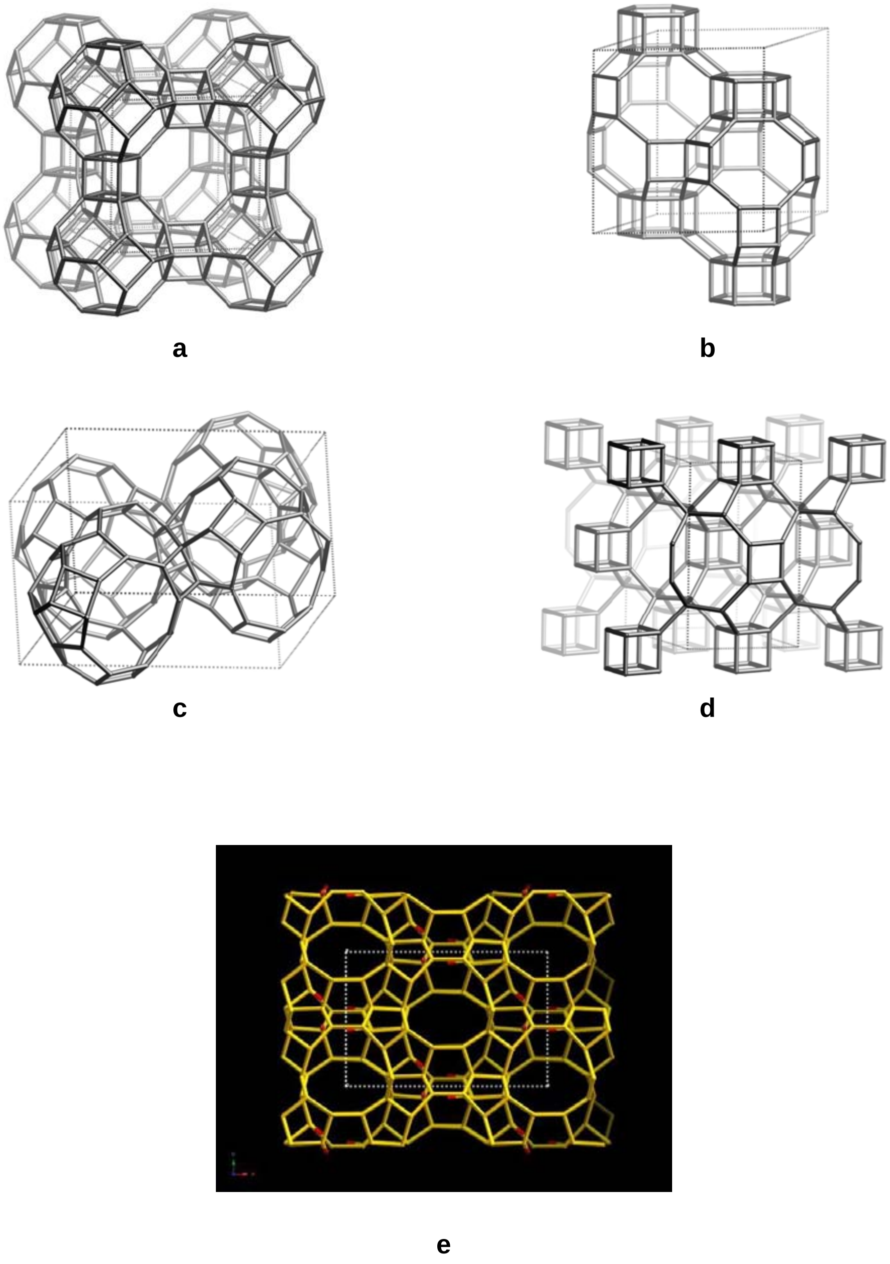

Figure 4.3 (a) LTA framework, viewed along the [001] axis; (b) CHA framework, viewed normal to the [001] axis; (c) STT framework, viewed normal to the [100] axis; (d) ITW framework, viewed along the [100] axis;[37] (e) -SVR framework, viewed along the [001] axis (courtesy of A. Burton, Chevron)

2. Results and Discussion

Using the vapor phase transport of the fluoride mineralizing agent, we created pure-silica zeolite films of each of the CHA, STT, ITW, and -SVR topologies on surface-modified (100) Si wafers (films of PSZ LTA were discussed in Chapter 3). XRD analysis showed that the calcined, and polished films have the correct structures (Figure 4.4), and that the films remained intact after polishing. FE SEM micrographs (Figure 4.5) of the calcined pure-silica films demonstrated that the films were polycrystalline, intergrown, and crack-free; these films were composed of small crystals on the order of a few microns to tens of microns in length. Micrographs of pure-silica CHA (Figure 4.5a), for instance, show 10-20 μm crystals with approximately square facets that are completely intergrown, while the pure-silica ITW crystals (Figure 4.5e) are frequently quite small (< 1 μm), and form intergrown, sphere-like aggregates that are themselves intergrown with neighboring aggregates. Interestingly, while the LTA film syntheses discussed in Chapter 3 tend to produce very regular crystals of its typical habit, the four film types generated here are composed of less regular crystals. The pure-silica STT films (Figure 4.5b) were synthesized using the same gel composition, SDA, and crystallization temperature as the previously reported films of PSZ CHA, whose structure has three-dimensional channels, as opposed to the two-dimensional structure of STT; for the STT films, however, the crystallization time was longer. For intermediate crystallization times (40 – 60 h), films composed of PSZ CHA and STT intergrowths could be formed (Figure 4.5c), although longer times would complete the phase transformation to STT. Mechanical polishing of the calcined PSZ STT and -SVR films (Figure 4.5d and Figure 4.5g, respectively), yielded films of 1.5 – 2.0 microns thickness (Figure 4.5h).

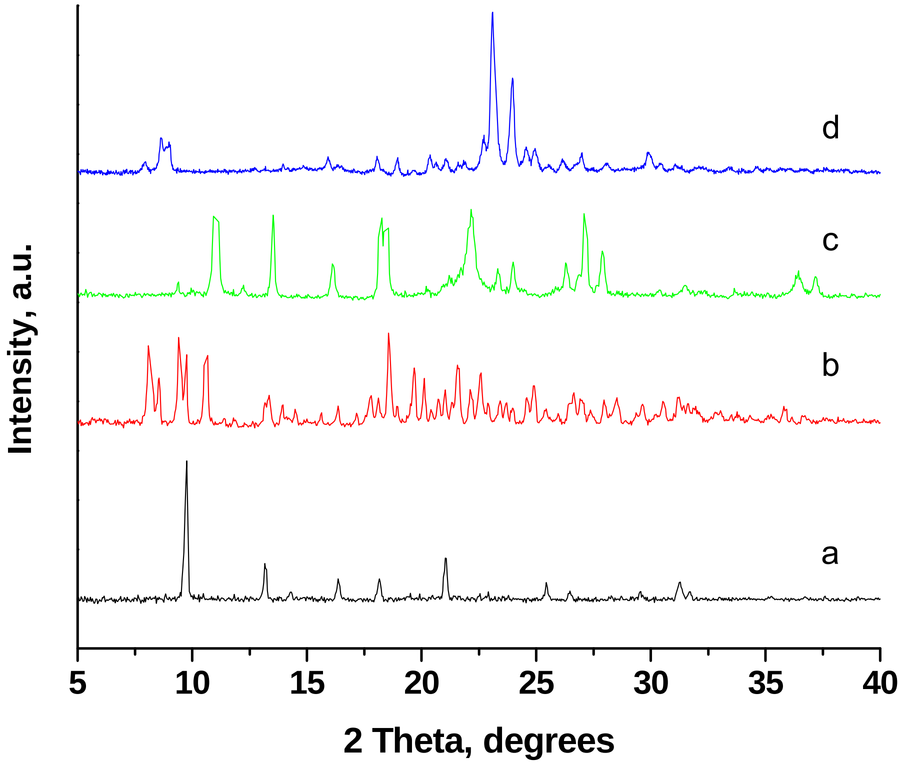

Figure 4.4 X-ray diffraction patterns of calcined and polished (a) PSZ CHA films on (100) Si; (b) PSZ STT films on (100) Si; (c) PSZ ITW films on (100) Si; (d) PSZ -SVR films on (100) Si

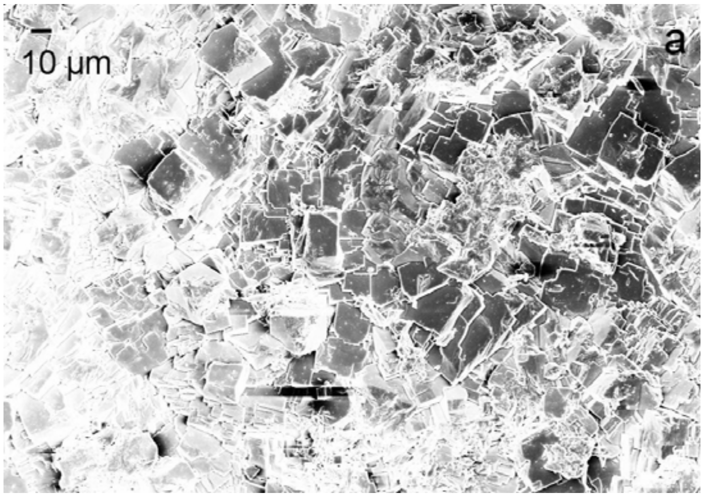
10 µm
a

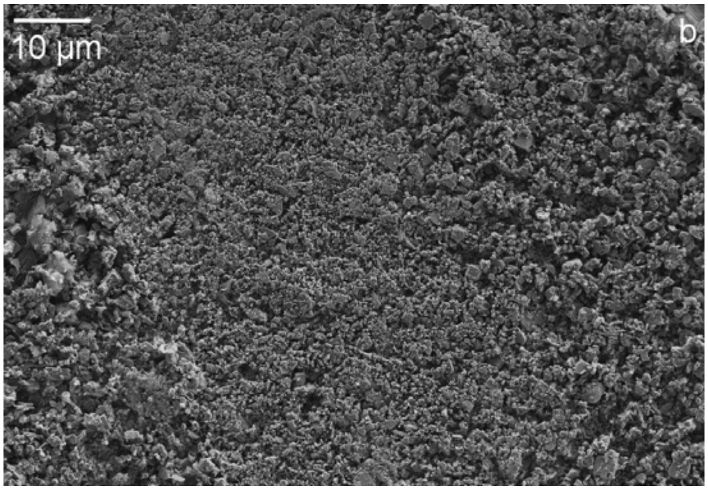
10 µm
b

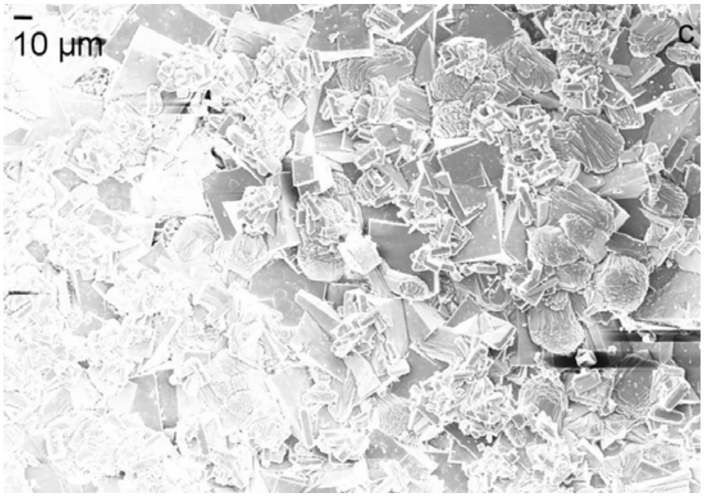
10 µm
c

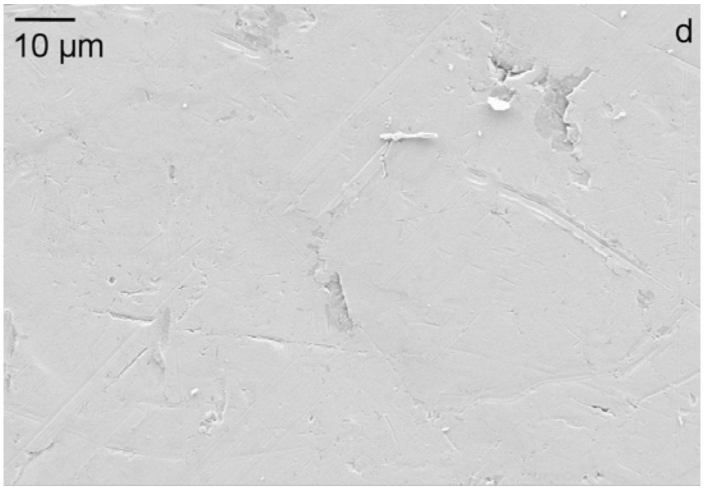
10 µm
d

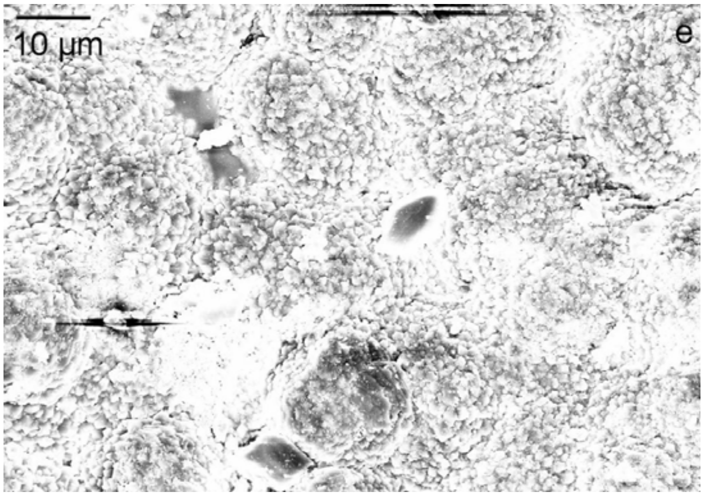
10 µm
e

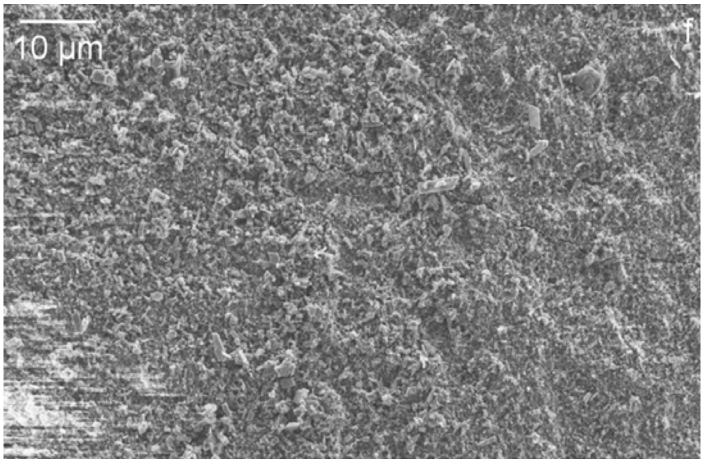
10 µm
f

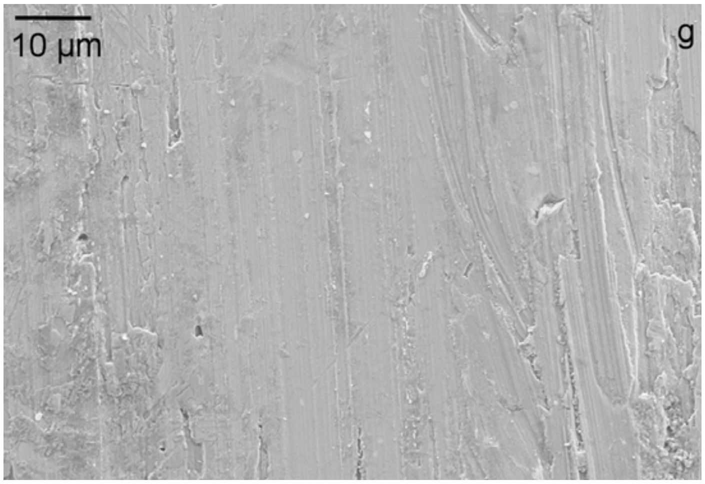

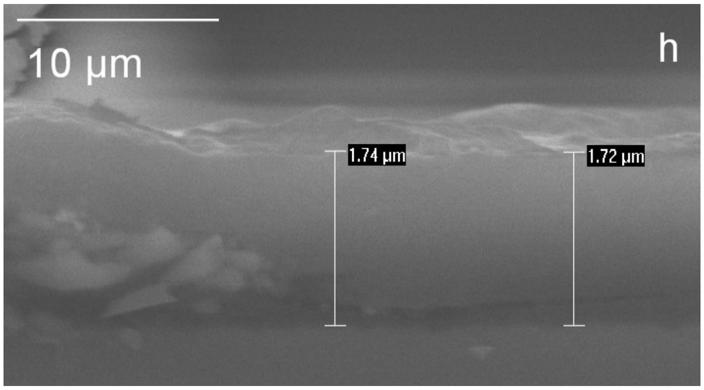

Figure 4.5 FE SEM micrographs of (a) surface of calcined PSZ CHA film; (b) surface of calcined PSZ STT film; (c) surface of PSZ CHA / STT intergrowth; (d) calcined, polished PSZ STT film; (e) surface of calcined PSZ ITW film; (f) surface of calcined PSZ -SVR film; (g) surface of calcined, polished PSZ -SVR film; (h) thin section of a typical PSZ STT film after mechanical polishing, showing ~ 1.7 μm thick film with variable height

The dielectric properties of the five pure-silica materials were investigated to determine their relevance for low-*k* applications. Initially, we attempted to measure the *k*-value using thin film, metal-insulator-metal, parallel-plate capacitance measurements using an LCR meter, as described earlier.[6] However, the results of these measurements were inconsistent, due to the variable thickness of the films, which led to metal-insulator-metal structures that were not perfectly parallel. This was caused by the limitations of the mechanical polishing equipment available rather than the materials themselves; we could not polish the samples with the precision necessary to create perfectly parallel structures. This was demonstrated via the capacitance measurements on the PSZ LTA thin films, which yielded a *k*-value of $k = 1.69$ ($\sigma = 0.18$). Here, an increase in film thickness of 20 nm over a 5 μm length of film (shown in Chapter 3) resulted in a standard deviation in the *k*-value measurements of 0.18. The theoretical *k*-value of PSZ LTA obtained from GULP (general utility lattice program) calculations at infinite frequency is 1.55. [7,38] Considering the range of errors inherent in the film measurements, the *k*-values obtained on the films in this study are in good agreement with those obtained from calculations. Comparison of the *k*-values from PSZ LTA films to PSZ *MRE ($k = 2.7$), PSZ BEA* ($k = 2.3$ and 2.07), and MFI ($k = 2.7$), that are obtained via *in situ* techniques that result in polycrystalline, intergrown, films whose porosity is solely due to the internal zeolite structure, shows a 37%, 26%, 18%, and 37% decrease in *k*, respectively (Figure 4.6). The *k*-value of the PSZ LTA film is the lowest obtained for any *in situ* synthesized polycrystalline PSZ film.

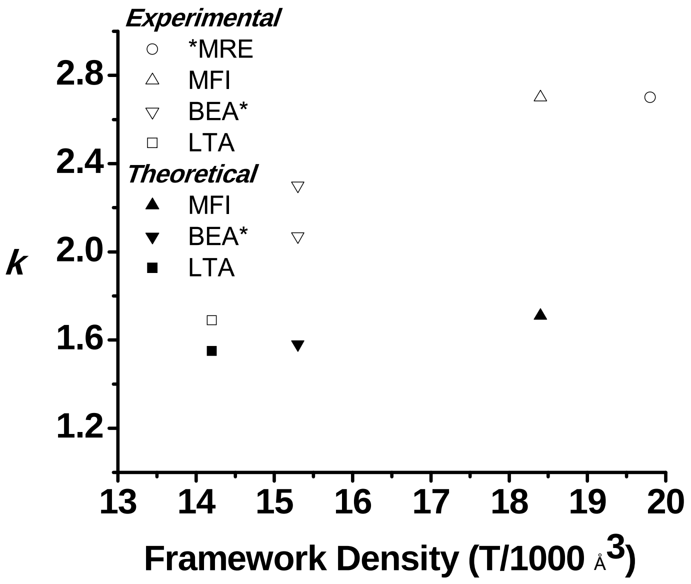

Figure 4.6 *k*-values obtained for PSZ thin film of *MRE, MFI, BEA*, and LTA topologies made by *in situ* (MFI and BEA*) and vapor phase transport methods (*MRE and LTA)

In order to avoid the problems mentioned earlier with parallel-plate capacitance measurements, and to evaluate the intrinsic *k*-values of the new film topologies, we instead utilized the Time-Domain Reflectometry method to analyze the dielectric properties of the powder generated during these film syntheses.[7] Using this method, we measured the dielectric constant of PSZ CHA, ITW, STT, and -SVR powder samples (Table 1; the dielectric constant of PSZ LTA powder was measured in a previous report[7]). For these measurements, the Bruggeman effective medium approximation, given by Equation 4.5, was used to calculate the dielectric constant of the zeolite crystals from the effective dielectric constant of the powder plus the air in the transmission line [7].

$$f_1 \frac{\kappa_1 - \kappa_e}{\kappa_1 + 2\kappa_e} + f_2 \frac{\kappa_2 - \kappa_e}{\kappa_2 + 2\kappa_e} = 0 \qquad \textbf{4.5}$$

In Equation 4.5, f_i symbolizes the volume fraction of components *i*, k_i the dielectric constant of component *i*, and k_e the effective (measured) dielectric constant of the mixture. The volume fraction of the components can be calculated from the mass of the loaded powder, the powder density, and the transmission line volume. In this case, we use k_1 as the dielectric constant of air, 1.0005, and k_2 as the dielectric constant of the measured powder material. The dielectric constant of the zeolites were obtained at a frequency of 2 GHz (shown in Table 4.1), from data of the effective dielectric constant determined over a range of frequencies, as shown in Figures 4.5 – 4.8. The *k*-value of PSZ LTA measured via Time Domain Reflectometry is in good agreement with the *k*-value measured via parallel-plate capacitance.[38]

Table 4.1 Dielectric constant (k) of various pure-silica zeolite powders measured at 2 GHz.

Sample	FD_{Si}	Channel Type	Smallest Ring Size	Largest Ring Size	Symmetry	*k* at 2 GHz
MFI[a]	18.4	3D	4	10	Orthorhombic	2.13
ITW	17.7	2D	4	8	Monoclinic	2.58
FER[a]	17.6	2D	5	10	Orthorhombic	2.01
-SVR	17.2	3D	4	10	Monoclinic	2.56
STT	17.0	2D	4	9	Monoclinic	3.22
CHA	15.1	3D	4	8	Rhombohedral	2.40
LTA[a]	14.2	3D	4	8	Cubic	1.62

[a] Dielectric constants reported in prior work [7]

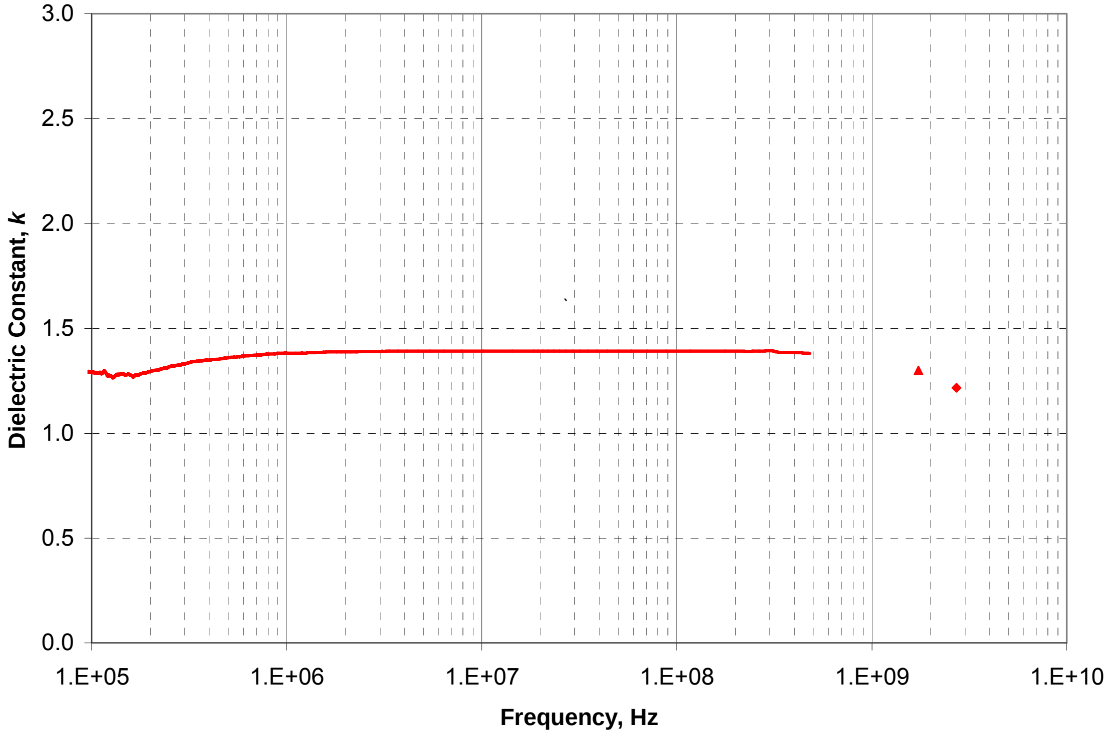

Figure 4.7 Effective dielectric constant of pure-silica CHA measured over a range of frequencies

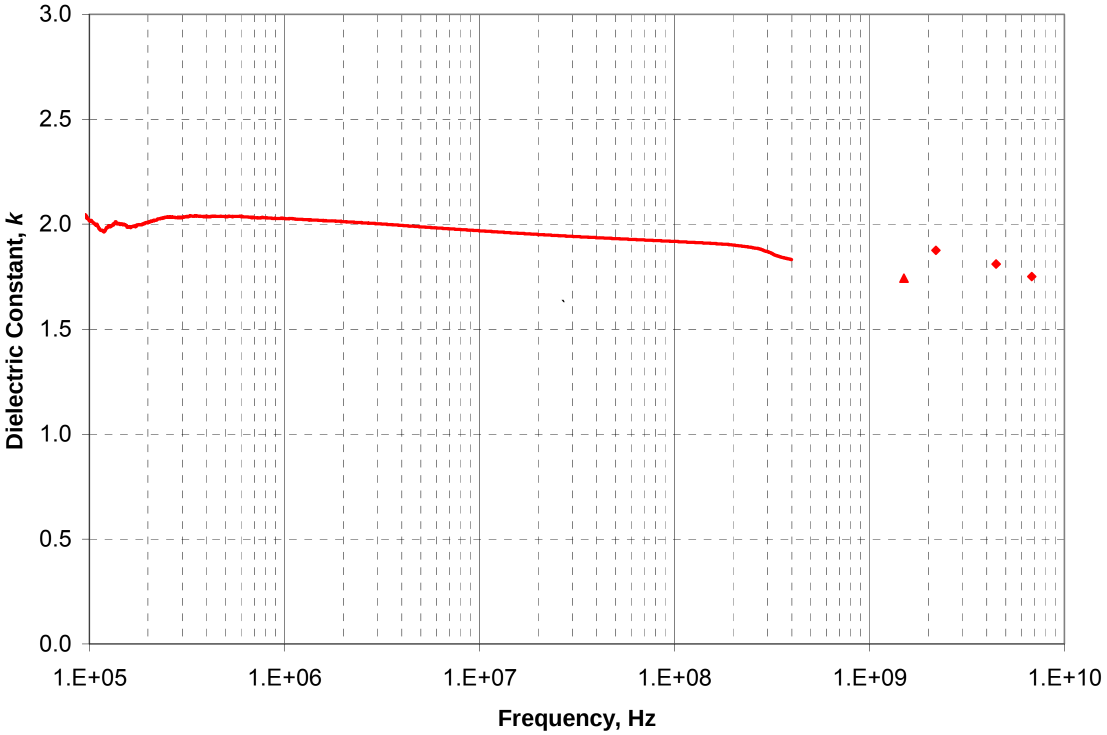

Figure 4.8 Effective dielectric constant of pure-silica STT measured over a range of frequencies

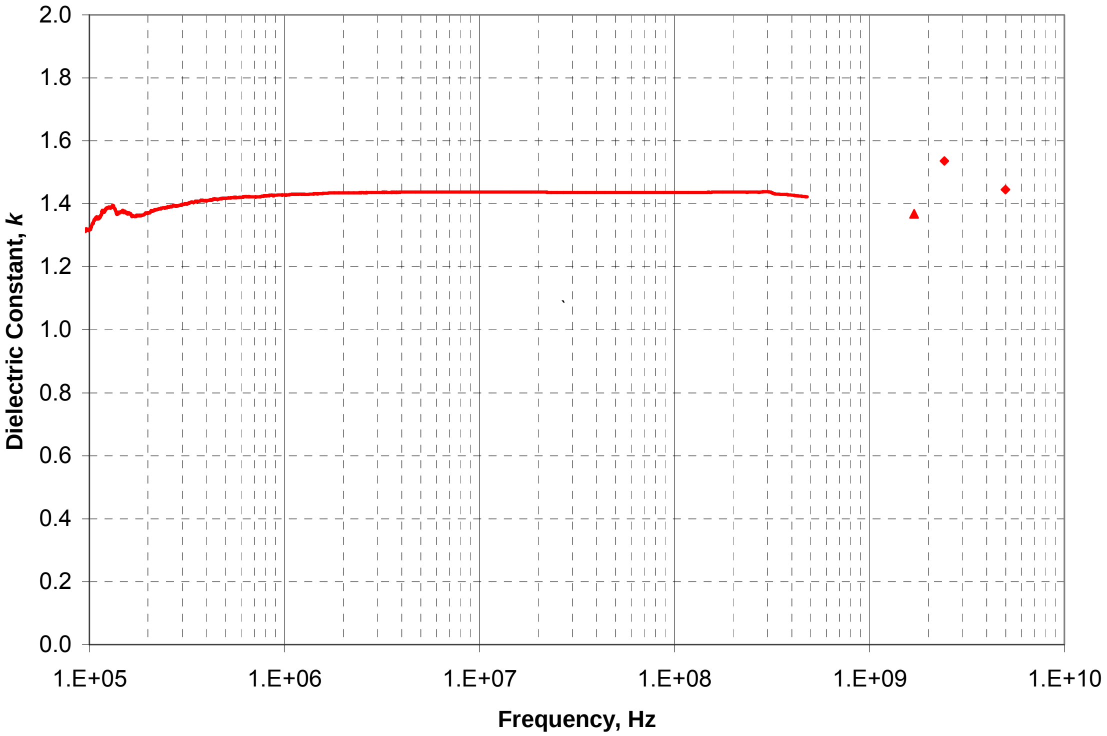

Figure 4.9 Effective dielectric constant of pure-silica ITW measured over a range of frequencies

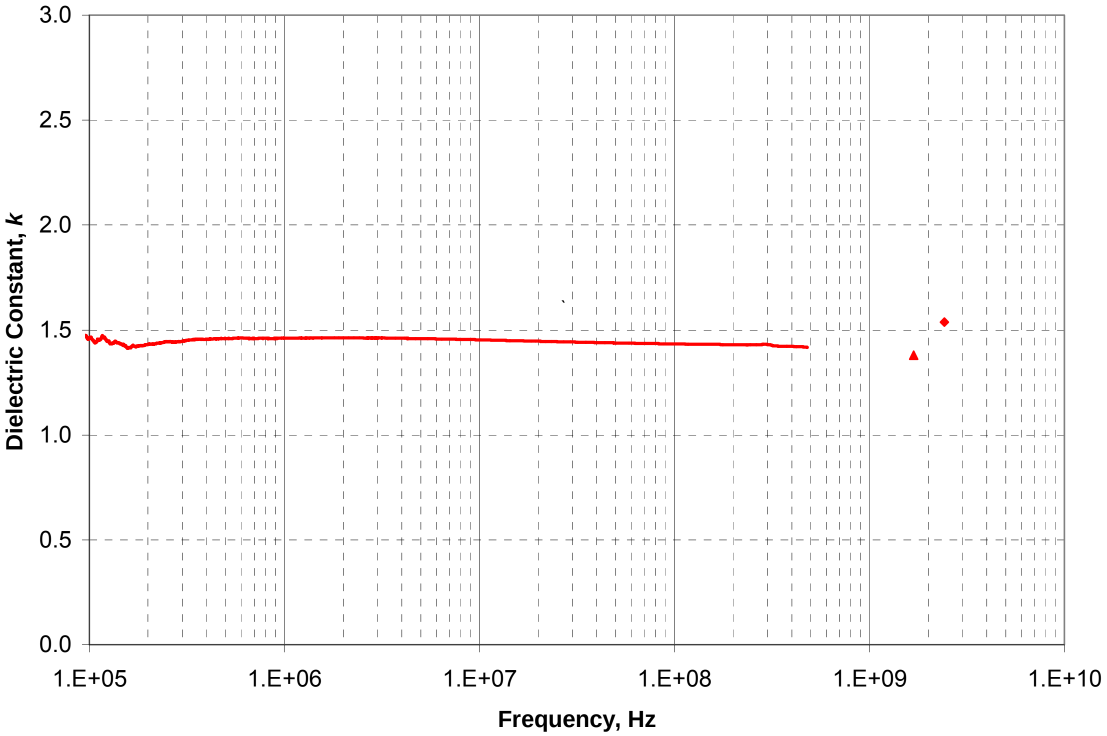

Figure 4.10 Effective dielectric constant of pure-silica -SVR measured over a range of frequencies

The *k*-values of these four PSZ topologies, along with the dielectric constants of PSZ LTA, FER, and MFI (all measured using TDR), are shown in Figure 4.11.[7] In the case of the PSZ ITW powder samples, we were unable to completely remove the organic SDA from the crystals, even with up to five cycles of calcination in air, resulting in very pale grey samples. The occlusion of organic molecules may result in a higher dielectric constant, because the internal void space of the sample is not fully open. The results of thermogravimetric analysis on the calcined, and prepared for TDR, powder samples demonstrate that the samples prepared as described each retain or adsorb while in storage very low amounts of water (< 1.0 % mass loss due to water adsorption up to 200 °C, and < 3.0 % mass loss overall up to 1000 °C). Figure 4.11 also shows the line that represents the Bruggeman effective medium correlation, which has been used as a guideline for the dielectric constant of solid materials (including zeolites). The Bruggeman correlation assumes that the intrinsic *k*-value of a material is the weighted average of the *k* from air in pores of the material, and the *k* from dense silica, as determined by the volume fraction of each. This implies that the measured *k* should be dependent entirely on the porosity of the zeolites; however, as Figure 4.11 shows, this is not the case. All the zeolites shown here fall below the line for the Bruggeman correlation, except for STT, which falls on the line, suggesting that their dielectric constants depend on pore structure in addition to the porosity. This is further shown by the ITW / FER / -SVR / STT series, whose framework densities all fall in the range 17.0 – 17.7. The smallest ring size for each of these materials is 4 for ITW, -SVR, and STT, while FER has a 5-ring as the smallest. Both the FER, and -SVR have 10-rings as their largest rings, although FER has only two-dimensional channels, as compared to the three-dimensional channels of -SVR. Interestingly, direct comparison between the *k*-values of the FER and ITW materials' *k*-values suggests that not only does a lower FD reduce the *k*-value of a sample, but so does the greater largest ring size in the FER material. Additionally, although the FD of -SVR is lower than that of FER, and has three-dimensional channels, its *k*-value is higher. However, in comparison to the *k*-value of STT, -SVR is lower. Like FER, STT has two-dimensional channels, but different ring sizes (4-rings at the smallest, and 9-rings at the largest). The differences in pore connectivity between STT and -SVR are likely the cause of the differences between their respective *k*-values. Further evaluations of the *k*-values from a symmetry perspective suggest that zeolites with a higher symmetry have a lower dielectric constant, as shown in Table 4.1, primarily because higher symmetry lattice arrangements of molecules lead to lower polarizability. The three zeolites with monoclinic symmetry (ITW, -SVR, and STT) all show higher *k*-values than the other materials. This may explain the distinct differences between the *k*-values of FER and ITW, for instance, whose pore architecture is similar in terms of framework density, and close in smallest and largest ring sizes, but different in terms of lattice symmetry. The comparatively high *k*-value of STT may then be a result of a combination of factors, including a high framework density, a two-dimensional pore channel system, and low symmetry. Additionally, the data shown in Figure 4.8 suggest that the STT sample may have had slight water adsorption, due to the slightly negative slope of the dielectric constant over the range of frequencies; materials with water adsorption generally show very steep declines in the dielectric constant as the frequency is increased. Perhaps most interesting is the nonlinear, although generally negative, dependence of *k*-values on FD. This indicates that, although porosity is the main factor in inducing a lower dielectric constant in porous silica, as compared to bulk silica, the structure of the porosity, as indicated by the ring size, micropore volume, and lattice symmetry, also plays a role in determining the *k*-value.

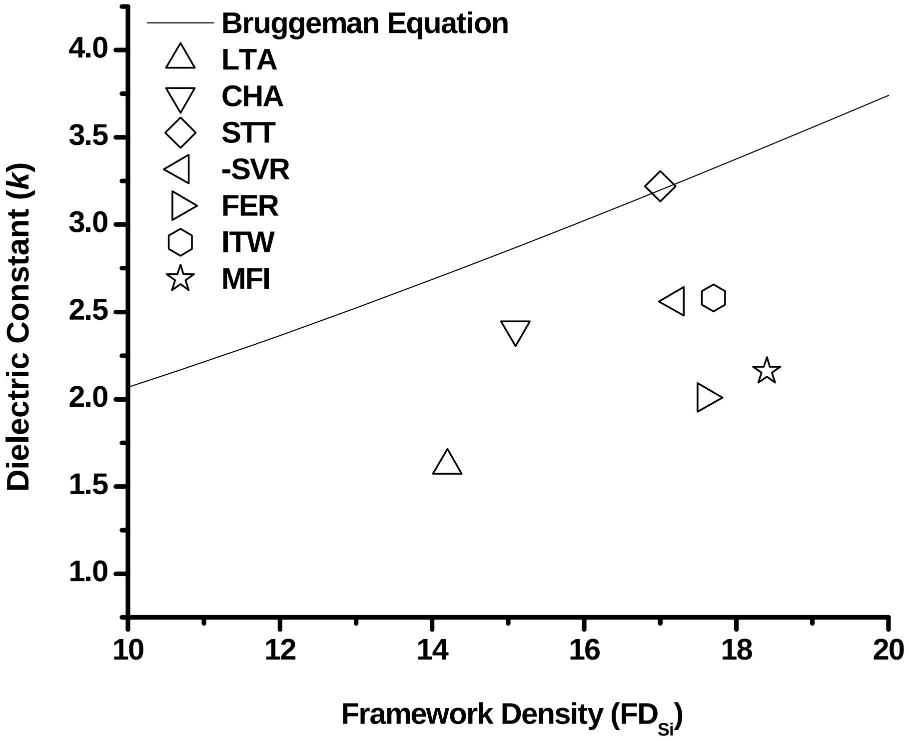

Figure 4.11 *k*-values obtained for fluoride-mediated, PSZ powders of MFI, ITW, FER, -SVR, STT, CHA, and LTA topologies via TDR

3. Conclusions

Application of the vapor phase transport of fluoride method to the pure-silica zeolite systems CHA, ITW, STT, and -SVR yielded thin films on surface-modified, (100) Si wafers. These films were continuous, polycrystalline, intergrown, and well-adhered to their substrates. The pure-silica ITQ-29 (LTA) films synthesized in Chapter 3 using this method were demonstrated to have a *k*-value of 1.69 via parallel-plate capacitance measurements, which is the lowest value experimentally obtained on any zeolite film. The pure-silica zeolite powders crystallized in conjunction with the film syntheses of these materials were examined via Time Domain Reflectometry at high frequencies to determine their dielectric properties, and compared to *k*-values of other pure-silica zeolites measured using this technique to evaluate if the reduction in their relative permittivity is solely the result of the introduction of porosity, or if other factors, such as pore structure, affect their *k*-value. These data demonstrate that the dielectric properties of zeolites are primarily a result of their porosities, but are also affected by their pore structures. Generally, materials with low framework density *and* high symmetry have low relative permittivities. Using this general relationship between the dielectric constant, and the porosity / pore structure of the zeolite, it is possible to tune the final values of the dielectric properties of the materials. For instance, the dielectric constant of these materials may be further reduced by the incorporation of porogens into the initial gel that is dip-coated onto the substrate; after crystallization and calcination, the continuous film will have a lower effective dielectric constant due to the presence of additional porosity. These properties make pure-silica zeolites excellent candidates for low-*k* materials.

4. Experimental

4.1 Synthesis of Structure-Directing Agent A (1,2,3-trimethylimidazolium hydroxide)

9.6 g of 1,2-dimethylimidazole (98%, Aldrich) was dissolved in 100 mL ethyl acetate (EMD). 20 g of CH_3I (99%, Aldrich) was added and the reaction mixture was stirred at room temperature under Ar for three days. The addition of CH_3I, followed by stirring for three days, was repeated once. The solution immediately produces white precipitate; this was collected via centrifugation. The solids so collected were washed copiously with diethyl ether (J. T. Baker), centrifuged again, decanted from the supernatant, and dried using a rotovap. The crude product was recrystallized from chloroform (EMD) at its boiling point and cold diethyl ether. White crystals of 1,2,3-trimethylimidazolium iodide were obtained after vacuum drying the resulting solid. The product (23.0 g, 96.6 mmol) was ion-exchanged from its iodide form to its hydroxide form by dissolution in 700 mL of DDI H_2O and stirring with 75 g of Bio-Rad AG1-X8 anion exchange resin for 24 h. The solution was then filtered and concentrated to 1 – 1.2 M concentration of the hydroxide form using a rotovap. The conversion from iodide to hydroxide was 85% based on titration of the resultant solution.

4.2 Synthesis of Structure-Directing Agent B (N,N,N-trimethyl-1-adamantylammonium hydroxide)

25 g of 1-adamantylamine (97%, Aldrich) was dissolved in 200 mL methanol (EMD). 33 g of potassium bicarbonate (99.7%, Aldrich) was added to the solution, which was then placed under an Ar atmosphere in an ice bath. 77.4 g of CH_3I was added to the solution,

and the reaction mixture was stirred for 3 days, slowly coming to room temperature. The solution was evaporated using a rotovap, and the product was extracted from the resulting solids with a large excess of chloroform. The solution was filtered to remove the potassium bicarbonate byproducts, and the solids were again washed with chloroform. The filtrate was dryed with magnesium sulfate (99%, Aldrich) until it no longer clumped in the solvent. The solution was filtered again to remove the magnesium sulfate. The solution was evaporated using a rotovap, the solids were washed with diethyl ether, and the solution was evaporated again using a rotovap. The crude product was recrystallized from a minimum of hot methanol at its boiling point. White crystals of N,N,N-trimethyl-1-adamantylammonium iodide were obtained after vacuum drying the resulting solid. The product (7.3 g, 22.7 mmol) was ion-exchanged from its iodide form to its hydroxide form by dissolution in 150 mL of DDI H_2O and stirring with 20 g of Bio-Rad AG1-X8 anion exchange resin for 24 h. The solution was then filtered and concentrated to 0.75 M concentration of the hydroxide form using a rotovap. The conversion from iodide to hydroxide was 95% based on titration of the resultant solution.

4.3 Synthesis of Structure-Directing Agent C (Hexamethylene-1,6-bis-(N-methyl-N-pyrrolidinium) hydroxide)

4.1 g of N-methylpyrrolidine (97%, Aldrich) was dissolved in 50 mL acetone (Fisher). 4.9 g of 1,6-dibromohexane (98%, Acros Organics) was added to the solution, and the resulting solution was stirred for three days. The solids produced were collected via centrifugation, washed with diethyl ether, centrifuged again, decanted from the supernatant, and dried using a rotovap. Crystals of hexamethylene-1,6-bis-(N-methyl-N-pyrrolidinium) bromide were obtained after vacuum drying the resulting solid. The product (3.7 g, 8.9 mmol) was ion-exchanged from its iodide form to its hydroxide form by dissolution in 20 mL of DDI H_2O and stirring with 10 g of Bio-Rad AG1-X8 anion exchange resin for 24 h. The solution was then filtered and concentrated to 0.23 wt % concentration of the hydroxide form using a rotovap. The conversion from iodide to hydroxide was 90% based on titration of the resultant solution.

4.4 Surface Modification of the Substrates

The low-resistivity (0.008 – 0.02 Ω cm), (100) silicon wafers (University Wafers) were modified to present Si-OH terminal groups on their surface by soaking in a pirahna-type etch solution, i.e., 10 mL H_2SO_4 (97%, J.T. Baker) : 40 mL H_2O_2 (30%, EMD) : 2 drops of HF (48%, Mallinckrodt), for 2 min, followed by 15 min in DDI H_2O.

4.5 Synthesis of Fluoride-Mediated, Pure-Silica Zeolite Films and Powder

Pure-silica precursor gels of ITW, CHA, STT, and -SVR were prepared in a Teflon® jar by hydrolyzing tetraethylorthosilicate (TEOS, 98%, Aldrich) in an aqueous solution of SDA (see Table 4.2 for gel compositions and reaction conditions). A 4 cm x 2 cm, previously modified substrate was then submerged in the gel. The precursor gel was stirred for 48 h, while covered with parafilm, at room temperature to ensure complete hydrolysis of TEOS. The submerged substrate was thereafter removed from the gel, and subjected to dip-coating up to five times in the hydrolyzed gel, with 30 min of drying on a Teflon® substrate holder at room temperature between coats. A Teflon® cap with two small holes drilled in it was screwed onto the jar containing the bulk precursor gel. The coated substrate, in its holder, and the enclosed bulk precursor gel were each placed inside a vacuum desiccator, and the ethanol and excess H_2O present in the bulk precursor gel and precursor film were evaporated. Evacuation for 48 h at room temperature yielded an amorphous precursor film and a solid (dry) bulk gel of molar composition of the appropriate final gel. If, after drying, too much H_2O had been removed, DDI H_2O was added to the jar to obtain the correct total gel mass. An aqueous solution of hydrofluoric acid (48%, Mallinckrodt) was added to the jar in molar ratio 0.50 HF / 1.0 SiO_2, and the sample was stirred with a Teflon® spatula. The dry bulk gel, followed by the coated substrate on an elevated Teflon® platform, was introduced into a Teflon®-lined Parr Autoclave. The crystallization of the bulk gel and the precursor films was carried out at conditions listed in Table 4.2. The reactor was removed from the oven and cooled. The bulk solids and the film were washed with 100 mL each of acetone (EMD) and DDI H_2O. The crystalline material was placed in an evaporating dish and dried for 24 hours in a 100 °C oven. The organic SDA was removed from the powder and film samples by calcination in air to the temperature given in Table 4.2 using a ramp rate of 1 °C / min, with pauses at 350 °C and 580 °C (for calcination temperatures over 580 °C) for 3 h each. The calcined films were mechanically polished using a Buehler EComet 3000 Polisher equipped with 0.05 μm Al_2O_3 polishing suspension and a 3 μm abrasive lapping film. To minimize water adsorption in the powder samples, after the powder was calcined, it was placed in a sealed vial and evacuated to 2×10^{-5} Torr overnight at 140 °C. The vial was then backfilled with dry argon and stored inside two Ziploc bags, each containing several grams of desiccant.

Table 4.2 Synthesis conditions for zeolite films and powders

Sample	Final Gel Composition	Crystallization Temperature	Crystallization Time	Calcination Temperature	Calcination Time @ T
ITW	1.0 TEOS / 0.5 SDA A / 0.5 HF / 3.0 H_2O	150 °C	10 days	650 °C	10 h
CHA	1.0 TEOS / 0.5 SDA B / 0.5 HF / 3.0 H_2O	150 °C (60 rpm)	40 h	580 °C	10 h
STT	1.0 TEOS / 0.5 SDA B / 0.5 HF / 3.0 H_2O	150 °C	3 – 10 days	580 °C	10 h
-SVR	1.0 TEOS / 0.5 SDA C / 0.5 HF / 3.0 H_2O	150 °C	20 days	595 °C	5 h

4.6 Characterization

The as-made and calcined zeolite powder and film samples were evaluated using X-ray diffraction (XRD). XRD was carried out on a Scintag XDS 2000 diffractometer operated at 40 kV and 40mA using Cu K_α radiation ($\lambda = 1.54056$ Å) and a solid-state Ge detector in the 2θ range of 2-55 at a step size of 0.5 ° / min. Thermogravimetric analysis (TGA) was performed on the calcined powder samples using a NETZSH STA 449C analyzer in air using an aluminum sample pan. All FE SEM was done on a LEO 1550 VP FE SEM at an electron high tension (EHT) of 10 kV using samples that were coated, using a metal sputtering coater, with 5 nm of Pt to minimize the effects of charging. EDS measurements were carried out using an Oxford INCA Energy 300 EDS system. The dielectric constants of the powder samples were obtained using time-domain reflectometry (TDR) carried out with a Tektronix TDS8200 equivalent time sampling oscilloscope and an Agilent E5071B vector network analyzer with a frequency range of 200 kHz – 8.5 GHz, coupled with a 50 Ω coaxial transmission (air) line from Maury

Microwave Corporation.[7] The dielectric constant of the calcined, polished, pure-silica LTA films on low-resistivity (100) Si was calculated from parallel-plate capacitance measurements obtained at a frequency of 1 MHz using an LCR meter under flowing dry argon to prevent accumulation of water in the sample, which has been shown to increase the dielectric constant value. For additional prevention of water adsoption, the surface of the pure-silica LTA films was capped using a vapor-phase silylation procedure described elsewhere to prevent water adsorption.[6] The capacitance measurements on the PSZ LTA films were carried out on metal-insulator-metal structures created by depositing, on the film, aluminum dots of diameter 1.62 mm, and on the backside of the silicon substrate, an aluminum layer. Four to five Al dots were usually deposited on each film sample, and their average *k* reported.

5. References

[1] *International Technology Roadmap for Semiconductors.* (2007).

[2] Maex, K. *et al.* Low dielectric constant materials for microelectronics. *J. Appl. Phys.* **93**, 8793-8841 (2003).

[3] Li, Z. J. *et al.* Mechanical and dielectric properties of pure-silica-zeolite low-k materials. *Angew. Chem.-Int. Edit.* **45**, 6329-6332 (2006).

[4] Lew, C. M. *et al.* Hydrofluoric-Acid-Resistant and Hydrophobic Pure-Silica-Zeolite MEL Low-Dielectric-Constant Films. *Langmuir* **25**, 5039-5044 (2009).

[5] Xiang, Y., Chen, X., Tsui, T. Y., Jang, J. I. & Vlassak, J. J. Mechanical properties of porous and fully dense low-kappa dielectric thin films measured by means of nanoindentation and the plane-strain bulge test technique. *J. Mater. Res.* **21**, 386-395 (2006).

[6] Wang, Z. B., Wang, H. T., Mitra, A., Huang, L. M. & Yan, Y. S. Pure-silica zeolite low-k dielectric thin films. *Adv. Mater.* **13**, 746-749 (2001).

[7] Sun, M. *et al.* Dielectric constant measurement of zeolite powders by time-domain reflectometry. *Microporous Mesoporous Mat.* **123**, 10 (2009).

[8] Lee, B. D. *et al.* Ultralow-k nanoporous organosilicate dielectric films imprinted with dendritic spheres. *Nat. Mater.* **4**, 147-U126 (2005).

[9] Chen-Yang, Y. W., Chen, C. W., Wu, Y. Z. & Chen, Y. C. High-performance circuit boards based on mesoporous silica filled PTFE composite materials. *Electrochemical And Solid State Letters* **8**, F1-F4 (2005).

[10] Loboda, M. J. New solutions for intermetal dielectrics using trimethylsilane-based PECVD processes. *Microelectron. Eng.* **50**, 15-23 (2000).

[11] Vitale, S. A. & Sawin, H. H. Etching of organosilicate glass low-k dielectric films in halogen plasmas. *J. Vac. Sci. Technol. A-Vac. Surf. Films* **20**, 651-660 (2002).

[12] Larlus, O. *et al.* Silicalite-1/polymer films with low-k dielectric constants. *Appl. Surf. Sci.* **226**, 155 (2004).

[13] Lin, Y. B., Tsui, T. Y. & Vlassak, J. J. Octamethylcyclotetrasiloxane-based, low-permittivity organosilicate coatings - Composition, structure, and polarizability. *J. Electrochem. Soc.* **153**, F144-F152 (2006).

[14] Long, T. M. & Swager, T. M. Molecular design of free volume as a route to low-kappa dielectric materials. *J. Am. Chem. Soc.* **125**, 14113-14119 (2003).

[15] Baklanov, M. R. & Maex, K. Porous low dielectric constant materials for microelectronics. *Philos. Trans. R. Soc. A-Math. Phys. Eng. Sci.* **364**, 201-215 (2006).

[16] Davis, M. E. Ordered porous materials for emerging applications. *Nature* **417**, 813-821 (2002).

[17] Yan, Y. & Wang, H. in *Encyclopedia of Nanoscience and Nanotechnology.* Vol. X, (H. S. Nalwa, ed.) 1-19 (American Scientific Publishers, 2003).

[18] Yan, Y., Wang, Z. & Wang, H. *Silica Zeolite Low-K Dielectric Thin Films.* U.S. Patent #6573131 (2003).

[19] Morgen, M. *et al.* Low dielectric constant materials for ULSI interconnects. *Annu. Rev. Mater. Sci.* **30**, 645-680 (2000).

[20] Corma, A., Rey, F., Rius, J., Sabater, M. J. & Valencia, S. Supramolecular self-assembled molecules as organic directing agent for synthesis of zeolites. *Nature* **431**, 287-290 (2004).

[21] Tiscornia, I. *et al.* Preparation of ITQ-29 (Al-free zeolite a) membranes. *Microporous Mesoporous Mat.* **110**, 303-309 (2008).

[22] Davis, M. E. *Zeolite Films for Low k Applications*. U.S. Patent # 7,109,130 B2.

[23] Chen, Y. L. *et al.* Synthesis and characterization of pure-silica-zeolite Beta low-k thin films. *Microporous Mesoporous Mat.* **123**, 45-49, doi:10.1016/j.micromeso.2009.03.022 (2009).

[24] Cho, Y. Pure Silica Zeolite Films Prepared by a Vapor Phase Transport Method. *Japanese Journal of Applied Physics. Parts 1 & 2* **47**, 8360-8363 (2008).

[25] Lew, C. M. *et al.* Pure-Silica-Zeolite MFI and MEL Low-Dielectric-Constant Films with Fluoro-Organic Functionalization. *Adv. Funct. Mater.* **18**, 3454-3460 (2008).

[26] Li, Z. J., Lew, C. M., Li, S., Medina, D. I. & Yan, Y. S. Pure-silica-zeolite MEL low-k films from nanoparticle suspensions. *J. Phys. Chem. B* **109**, 8652-8658 (2005).

[27] Liu, Y., Sun, M. W., Lew, C. M., Wang, J. L. & Yan, Y. S. MEL-type pure-silica zeolite nanocrystals prepared by an evaporation-assisted two-stage synthesis method as ultra-low-k materials. *Adv. Funct. Mater.* **18**, 1732-1738 (2008).

[28] Mitra, A. *et al.* Synthesis and evaluation of pure-silica-zeolite BEA as low dielectric constant material for microprocessors. *Ind. Eng. Chem. Res.* **43**, 2946-2949 (2004).

[29] Hu, L. L., Wang, J. L., Li, Z. J., Li, S. & Yan, Y. S. Interfacial adhesion of nanoporous zeolite thin films. *J. Mater. Res.* **21**, 505-511 (2006).

[30] Hunt, H. K., Lew, C. M., Sun, M., Yan, Y. & Davis, M. E. Pure-Silica Zeolite Thin Films by Vapor Phase Transport of Fluoride for Low-*k* Applications. *Microporous Mesoporous Mat.* (In Press).

[31] Diaz-Cabanas, M. J., Barrett, P. A. & Camblor, M. A. Synthesis and structure of pure SiO2 chabazite: the SiO2 polymorph with the lowest framework density. *Chem. Commun.*, 1881-1882 (1998).

[32] Yang, X. B., Camblor, M. A., Lee, Y., Liu, H. M. & Olson, D. H. Synthesis and crystal structure of As-synthesized and calcined pure silica zeolite ITQ-12. *J. Am. Chem. Soc.* **126**, 10403-10409 (2004).

[33] Baerlocher, C. *et al.* Ordered silicon vacancies in the framework structure of the zeolite catalyst SSZ-74. *Nat. Mater.* **7**, 631-635 (2008).

[34] Camblor, M. A. *et al.* A synthesis, MAS NMR, synchrotron X-ray powder diffraction, and computational study of zeolite SSZ-23. *Chem. Mater.* **11**, 2878-2885 (1999).

[35] Caro, J. & Noack, M. Zeolite membranes - Recent developments and progress. *Microporous Mesoporous Mat.* **115**, 215-233 (2008).

[36] Barrett, P. A. *et al.* ITQ-12: a new microporous silica polymorph potentially useful for light hydrocarbon separations. *Chem. Commun.*, 2114-2115 (2003).

[37] *Database of Zeolite Structures*. http://www.iza-structure.org/databases/ (2009).

[38] Sun, M. *et al.* Dielectric Constant Measurement of Zeolite Powders by Time Domain Reflectometry. *Microporous Mesoporous Mat.* (2009).